PAPER

Synthesis and anticancer activity of cyclometalated Pt(II) neutral complexes containing curcumin as a bioactive ancillary ligand†

Eugenia Giorno, [‡][a] Giorgio Facchetti, [‡][b] Nicolas Godbert, [a,c] Giuseppe Di Maio,[a] Massimo La Deda, [a,c,d] Giulia Coffetti,[b] Isabella Rimoldi, [*][b] Valentina Coccè,[e] Luisa Doneda,[e] Giulio Alessandri,[e] Francesca Paino,[e] Augusto Pessina[e] and Iolinda Aiello [*][a,c,d]

A novel series of cyclometalated platinum(II) complexes of curcumin, [(C^N)Pt(curc)] **1–5**, was synthesized *via* a microwave-assisted procedure, using NEt_3 as the base, which offers a safer and more efficient alternative to traditional synthetic methods. The complexes were obtained in high yields and fully characterized through spectroscopic and analytical techniques. Structural and spectroscopic data confirmed the coordination of curcumin to the Pt(II) center, with notable shifts in IR and NMR signals supporting metal–ligand interactions. Lipophilicity studies revealed log P values ranging from 3.15 to 3.76, consistent with favorable membrane permeability and drug-likeness. Photophysical characterization showed that all complexes exhibited broad absorption bands with LMCT and $\pi-\pi^*$ transitions and dual fluorescence emission bands, indicating the presence of coordinated species. Over time, a slow release of curcumin in solution was detected, although complexes remained stable under physiological conditions for at least 72 h, as confirmed by absorption studies. The antiproliferative activity of complexes **1–5** was initially screened on human fibroblasts, leading to the selection of complexes **3**, **4** and **5** for further evaluation on cancer cell lines. Complexes **4** and **5** showed notable cytotoxicity, particularly against SK-ES1 (Ewing's sarcoma), with IC_{50} values of 15.4 μM and 13.9 μM, respectively. These compounds maintained significant activity over 72 h, aligning with their spectroscopic stability. Given their potency, selectivity and lack of photoactivation requirement, complexes **4** and **5** emerged as promising candidates for the treatment of Ewing's sarcoma.

Introduction

Curcumin, H(curc), is a bright yellow pigment and represents the most significant constituent of turmeric (*Curcuma longa*),

[a]MAT-InLAB, LASCAMM CR-INSTM, Unità INSTM della Calabria, Dipartimento di Chimica e Tecnologie Chimiche, Università della Calabria, 87036 Arcavacata di Rende (CS), Italy. E-mail: iolinda.aiello@unical.it
[b]Università degli Studi di Milano, Dipartimento di Scienze Farmaceutiche, Via Venezian 21, 20133 Milan, Italy
[c]LPM-Laboratorio Preparazione Materiali, Star-Lab, Università della Calabria, 87036 Arcavacata di Rende (CS), Italy
[d]CNR NANOTEC-Istituto di Nanotecnologia UOS Cosenza, 87036 Arcavacata di Rende (CS), Italy
[e]CRC StaMeTec, Department of Biomedical, Surgical and Dental Sciences, University of Milan, 20122 Milan, Italy
†Electronic supplementary information (ESI) available: Experimental details: synthesis of complex **V**, NMR spectra, emission and excitation spectra of **H(curc)** and complexes **1–5**, photophysical characterization of **1** in a dilute solution, and log P value. See DOI: https://doi.org/10.1039/d5dt01323b
‡These authors contributed equally to this work.

which belongs to the ginger family. The interest in H(curc) stems from the multitude of medicinal properties related to its chemical structure, supporting a wide spectrum of therapeutic actions such as anti-inflammatory, antibacterial, antiviral, antifungal, antidiabetic, anticoagulant, hepatoprotective, anti-ulcer, hypotensive, and hypocholesterolemic.[1–5] Structurally, H(curc) comprises an unsaturated diketone moiety, two feruloyl groups and a seven-carbon linker. As with any β-diketone, the methylene group is easily prone to deprotonation and enolate formation, thus acquiring Michael acceptor ability and undergoing nucleophilic addition with target macromolecules.[6,7] While its antioxidant activity is mainly ascribed to the phenolic groups, the carbon linker enables hydrophobic interactions with proteins.[8,9] For these reasons, H(curc) is an attractive agent to be investigated in combination with other active species for the development of dual drug strategies.[10] Due to its unsaturated keto–enol moiety as a chelating agent, H(curc) is able to interact with many different metal ions.[11] Metal complexation, indeed, has been proved to

be an advantageous strategy to enhance its low bioavailability and pharmacokinetic instability for appropriate uptake at the cellular level.[12–14] Metal coordination, for example with Zn(II), Cu(II), Fe(II), Mn(II), Mg(II), Pt(II), Ru(II) and Pd(II), is responsible for significant structural changes in H(curc) and although it is able to bind to DNA *via* groove binding as a free ligand, the metallo-conjugate features additional binding ability comprising electrostatic interactions and intercalation.[14–16] As anticancer agents, the main effect of curc-metal chelates concerns antiproliferative and antimetastatic activity *via* mitochondrial pathways, the inhibition of angiogenesis by modulating the activity of NF-kB and the inhibition of carcinogenesis and tumour growth through free-radical scavenging properties.[17] Considering these interesting aspects of curcumin and the possibility of using it as a bioactive metal chelating ligand, different research studies have been reported underlining the use of these complexes as promising drugs towards both cisplatin-sensitive and resistant cells.[18,19] In addition, H(curc) coordination to a metal ion makes the corresponding complexes potentially photocytotoxic against a variety of cancer cells. H(curc) indeed shows an intense absorption band in the visible region at around 430 nm, thereby conferring useful photosensitizing properties.[20,21] The production of cytotoxic reactive oxygen species (ROS) by its photoactivated excited triplet state is well documented in the literature,[22,23] and is enhanced upon coordination to a heavy metal cation, such as Cu(II) or Zn(II).[18,19,24] Moreover, its emission at green wavelengths enables cellular tracking of curc–metal conjugates, paving the way for the preparation of theragnostic drugs. In this context, the Chakravarty group reported the synthesis of Platicur [Pt(cur)(NH₃)₂(NO₃)], a photoactivatable prodrug able to release both cisplatin and curcumin in a controlled manner upon visible light activation.[25] Platinum conjugation was shown to overcome H(curc) hydrolytic instability, thus leading to its localization in the cytosol of cancer cells where ROS species could be generated, and concurrently, the photorelease of H(curc) makes the "Pt(NH₃)₂" species available for DNA crosslink formation. Indeed, the lower cytotoxicity exhibited by Platicur in the dark showed the possibility to generate a new class of anticancer agents *via* light activation.[26–28] In order to develop increasingly potent and specific cytotoxic metal complexes,[29] cyclometalated complexes bearing photosensitizer chelating (C^N) ligands have attracted much attention due to their interesting biological and photoluminescence properties.[30] The long-lived triplet state offered by this class of metal complexes has been extensively exploited for achieving chemical and photostability in the biological environment, making them particularly suitable for real-time imaging and ROS generation.[28,31,32] Thus, by merging the advantageous photophysical properties of cyclometalated Pt(II) complexes with the biological properties of H(curc), in this study, we reported the synthesis and photophysical characterization of five novel orthometalated curc-Pt(II) complexes[33] and their anticancer activity evaluation against three different cancer cell lines, namely triple-negative breast cancer (MDA-MB 231),[34,35] osteosarcoma (SK-ES1),[36,37] and melanoma (M20).[38–40]

Experimental section

Materials and physical measurements

All commercially available chemicals were purchased from Merck or Alfa Aesar and used without further purification.

Precursor Pt(II) complexes, **[(ppy)Pt(H(ppy))(Cl)]** (**I**),[41] **[(ppy-F)Pt(H(ppy-F))(Cl)]** (**II**),[42] **[(bzq)Pt(H(DMSO))(Cl)]** (**III**)[43] and **[(tpy)Pt(DMSO)(Cl)]** (**IV**),[41] were synthesized as already reported.

The synthesis of the **[(pq)Pt(DMSO)(Cl)]** precursor complex (**V**) is reported in the ESI.†

The microwave assisted syntheses were carried out using a CEM Discover Synthesis Unit (CEM Corp., Matthews, NC) following the procedure reported in the literature.[41,44]

IR spectra (KBr pellets) were recorded on a PerkinElmer Spectrum 100 FT-IR spectrometer. ¹H-NMR and ¹³C-NMR spectra were recorded on a Varina VNMRS-400 spectrometer and calibrated using residual undeuterated solvent as the internal reference. Elemental analyses were performed with a PerkinElmer 2400 analyser CHNS/O. Melting points were determined with a Leica DMLP polarizing microscope equipped with a Leica DFC280 camera and CalCTec (Italy) heating stage.[45] Analyses (MS) were performed by using a Thermo Finnigan (MA, USA) LCQ. An Advantage system MS spectrometer with an electrospray ionisation source and an 'Ion Trap' mass analyser was used. The MS spectra were obtained by direct infusion of a sample solution in methanol under ionisation.

Spectrofluorimetric grade solvents were used for the photophysical investigations in solution, at room temperature. A PerkinElmer Lambda 900 spectrophotometer was utilized to obtain the UV/Vis absorption spectra, using quartz cuvettes of 1 cm path length. Steady-state emission spectra were recorded on a Horiba Jobin Yvon Fluorolog 3 spectrofluorimeter, equipped with a Hamamatsu R-928 photomultiplier tube. Time-resolved measurements were performed using the time-correlated single-photon counting (TCSPC) option on the Fluorolog 3. A Nanoled laser operating at 379 nm (FWHM 750 ps) with a repetition rate of 1 MHz was used to excite the sample. Excitation sources were mounted directly on the sample chamber at 90° to a single-grating emission monochromator (2.1 nm mm⁻¹ dispersion; 1200 grooves per mm) and collected with a TBX-04-D single-photon-counting detector. The experimental setup is accurately reported. The photons collected at the detector are correlated to the excitation pulse using a time-to-amplitude converter (TAC). Signals were collected using an IBH Data Station Hub photon-counting module, and data analysis was performed using the commercially available DAS6 software (HORIBA Jobin Yvon IBH). Goodness of fit was assessed by minimizing the reduced chi-squared function (χ^2) and visual inspection of the weighted residuals. The solid-state measurements were made in a front-face configuration using polycrystalline samples between quartz coverslips.[44]

General procedures for the synthesis of [(C^N)Pt(curc)] complexes, 1–5. In 20 mL of degassed methanol, H(curc) (1.5 eq.)

was solubilized and NEt_3 (1.5 eq.) was added. Successively, the corresponding precursor complexes, I–V, (1 eq.) were added. In the microwave oven, the reaction mixture was irradiated at 150 W and 65 °C for 12 min using a dynamic method.[43] The solvent was concentrated under vacuum and ethyl ether was added. The obtained solid was filtered off and washed with water and ethyl ether.

[(ppy)Pt(curc)], 1. Precursor complex I (112 mg, 0.24 mmol) was reacted with H(curc) (134 mg, 0.36 mmol) and NEt_3 (36.7 mg, 0.36 mmol), affording an orange solid. Yield 80% (267 mg). M.p. 242 °C dec.; $C_{32}H_{27}NO_6Pt$ (MW = 716.64): Anal. calcd: C, 53.63; H, 3.80; N, 1.95%; found: C, 53.61; H, 3.79; N, 1.98%. MS (ESI): m/z 717.15 $[M + H]^+$; FT-IR (KBr) ν_{max}/cm^{-1} 3435s (OH), 3042w (CH aromatic), [2963w, 2848w] (CH aliphatic), 1625m (C=C curc), 1608m (C=C ppy), 1595m (C=O), 1506vs, 1448m, 1419m, 1262m, 1178m, 1120m, 1032m, 964m, 851w, 817w, 741m, 610w, 561w; ^{1}H-NMR (300 MHz; DMSO-d_6; TMS) δH/ppm 9.13 (d, 1H, J_{HH} = 6 Hz, H^1), 8.11–8.03 (m, 2H), 7.80–7.63 (m, 4H), 7.51–7.46 (m, 1H), 7.39 (d, J_{HH} = 9 Hz, 2H), 7.30–7.23 (m, 2H), 7.08 (m, 4H), 6.89–6.73 (m, 4H), 5.97 (s, 1H, H^a), 3.88 (s, 6H, –OCH$_3$). ^{13}C NMR (75 MHz, DMSO-d_6; TMS) δC/ppm 177.40, 167.72, 149.40, 149.28, 148.68, 145.24, 139.79, 139.66, 139.35, 138.55, 127.68, 125.77, 125.02, 123.88, 123.23, 123.08, 116.34, 111.60, 111.29, 56.28.

[(ppy-F)Pt(curc)], 2. Precursor complex II (120 mg, 0.20 mmol) was reacted with H(curc) (108 mg, 0.30 mmol) and NEt_3 (29.8 mg, 0.30 mmol) to afford an orange solid; yield 56% (84 mg); m.p. >250 °C; $C_{32}H_{25}F_2NO_6Pt$ (MW = 752.62): Anal. calcd: C, 51.07; H, 3.35; N, 1.86%; found: C, 51.05; H, 3.32; N, 1.85%; MS (ESI): m/z 753.09 $[M + H]^+$; FT-IR (KBr) ν_{max}/cm^{-1} 3424m (OH), 3011w (CH aromatic), 2940w (CH aliphatic), 1625m (C=C curc), 1607m (C=O), 1505vs, 1405m, 1296m, 1262m, 1180w, 1122m, 964m, 851m, 812m, 777w, 705w, 611w; ^{1}H-NMR (300 MHz; DMSO-d_6; TMS) δH/ppm 9.20 (d, 1H, J = 3 Hz, H^1), 8.17 (t, J = 9 Hz, 1H), 8.01 (d, J = 9 Hz, 1H), 7.78 (d, J = 18 Hz, 1H), 7.63–7.53 (m, 2H), 7.39 (d, J = 15 Hz, 2H), 7.28 (d, J = 12 Hz, 1H), 7.17–7.13 (m, 2H), 6.96 (t, J = 9 Hz, 1H), 6.90–6.78 (m, 4H), 6.02 (s, 1H, H^a), 3.88 (s, 6H, –OCH$_3$). ^{13}C NMR (75 MHz, DMSO-d_6; TMS) δC/ppm 177.54, 176.06, 149.41, 148.60, 140.50, 139.86, 138.85, 127.54, 127.45, 125.23, 123.30, 116.27, 111.52, 110.99, 108.90, 101.38, 56.19.

[(bzq)Pt(curc)], 3. Precursor complex III (132 mg, 0.27 mmol) was reacted with H(curc) (150 mg, 0.42 mmol) and NEt_3 (41 mg, 0.42 mmol) to afford an orange solid; yield 70% (140 mg); m.p. 248 °C dec.; $C_{34}H_{27}NO_6Pt$ (MW = 740.67): Anal. calcd: C, 55.13; H, 3.67; N, 1.89%; found: C, 53.14; H, 3.69; N, 1.68%; MS (ESI): m/z 741.52 $[M + H]^+$; FT-IR (KBr) ν_{max}/cm^{-1} 3467s (O–H), 3035w (CH aromatic), [2964m, 2921m] (CH aliphatic), 1622s (C=C curc), 1595m (C=O), 1584s, 1515w, 1494m, 1406w, 1311m, 1259s, 1183m, 1112s, 1078m, 1017m, 850m, 802s, 709w, 661w, 461w; ^{1}H-NMR (300 MHz; DMSO-d_6; TMS) δH/ppm 9.36 (d, J = 6 Hz, 1H, H^1), 8.68 (d, J = 9 Hz, 1H), 7.94–7.72 (m, 6H), 7.68–7.63 (m, 2H), 7.44 (d, J = 12 Hz, 2H), 7.33–7.24 (m, 2H), 6.93–6.80 (m, 4H), 6.02 (s, 1H, H^a), 3.89 (s, 6H, –OCH$_3$). ^{13}C NMR (75 MHz, DMSO-d_6; TMS) δC/ppm 177.22, 175.48, 157.09, 149.32, 149.21, 148.66, 148.62, 147.26, 141.80, 139.64, 138.83, 138.49, 136.86, 133.22, 129.42, 129.08, 128.43, 127.78, 126.70, 125.71, 124.93, 124.05, 123.62, 123.31, 123.15, 122.28, 121.73, 121.54, 116.30, 111.83, 111.47, 111.21, 106.24, 56.23.

[(tpy)Pt(curc)], 4. Precursor complex IV (80 mg, 0.17 mmol) was reacted with H(curc) (94 mg, 0.26 mmol) and NEt_3 (26 mg, 0.26 mmol), affording an orange solid; yield 40% (49 mg); m.p. 216 °C; $C_{30}H_{25}NO_6PtS$ (MW = 722.67): Anal. calcd: C, 49.86; H, 3.49; N, 1.94%; found: C, 49.85; H, 3.50; N, 1.97%; MS (ESI): m/z 723.73 $[M + H]^+$; FT-IR (KBr) ν_{max}/cm^{-1} 3270sh (OH), 3005w (CH aromatic), [2937w, 2840w] (CH aliphatic), 1625m (C=C curc), 1606m, 1595m (C=O), 1505vs, 1416w, 1262m, 1179m, 1120m, 128m, 990w, 963w, 885w, 842w, 815w, 756w; 1H-NMR (300 MHz; DMSO-d_6; TMS) δH/ppm 8.94 (d, J = 6 Hz, 1H, H^1), 7.94 (t, J = 6 Hz, 1H), 7.77–7.72 (m, 2H), 7.64–7.49 (m, 2H), 7.37 (d, J = 12 Hz, 2H), 7.29–7.18 (m, 4H), 6.84–6.71 (m, 4H), 5.95 (s, 1H, H^a), 3.85 (s, 6H, –OCH$_3$). ^{13}C NMR (75 MHz, DMSO-d_6; TMS) δC/ppm 176.90, 175.23, 163.39, 149.30, 149.16, 148.59, 144.34, 140.40, 139.47, 138.53, 127.71, 125.60, 123.25, 122.94, 116.27, 111.39, 56.21.

[(pq)Pt(curc)], 5. Precursor complex V (108 mg, 0.21 mmol) was reacted with H(curc) (120 mg, 0.32 mmol) and NEt_3 (32 mg, 0.32 mmol) to yield a light brown solid; yield 30% (25 mg); m.p. 197 °C; $C_{36}H_{29}NO_6Pt$ (MW = 766.70): Anal. calcd: C, 53.40; H, 3.81; N, 1.83%; found: C, 53.42; H, 3.82; N, 1.84%; MS (ESI): m/z 767.15 $[M + H]^+$; FT-IR (KBr) ν_{max}/cm^{-1} 3426br (OH), 3005w (CH aromatic), 2963w (CH aliphatic), 1623m (C=C curc), 1591m (C=O), 1509vs, 1465w, 1293m, 1262m, 1166m, 1033w, 962w, 809w, 759w; ^{1}H-NMR (300 MHz; DMSO-d_6; TMS) δH/ppm 9.66 (d, J = 6 Hz, 1H, H^1), 8.67 (d, J = 6 Hz, 1H), 8.24 (d, J = 9 Hz, 1H), 8.12 (d, J = 9 Hz, 1H), 7.98 (t, J = 6 Hz, 1H), 7.88 (d, J = 6 Hz, 1H), 7.78–7.65 (m, 4H), 7.39–7.08 (m, 6H), 6.94–6.76 (m, 4H, H), 6.06 (s, 1H, H^a), 3.88 (s, 6H, –OCH$_3$). ^{13}C NMR (75 MHz, DMSO-d_6; TMS) δC/ppm 179.93, 177.09, 176.33, 149.41, 149.00, 140.61, 138.79, 131.91, 131.36, 128.41, 127.61, 127.35, 126.51, 124.96, 123.76, 117.61, 56.25.

Log P_{ow} determination

RP-HPLC analysis was performed to correlate the hydrophobicity of the complexes with their retention time. The chromatograms were analysed using a reversed-phase HPLC column (Partisil C18-ODS), at 25 °C, using KI as the internal standard and water/methanol in an 80/20 ratio in the presence of 15 mM HCOOH as the mobile phase (flow rate: 1 mL min^{-1} and λ = 210 nm). The calibration curve was realized in comparison with reference compounds (*i.e.*, cisplatin, carboplatin and oxaliplatin).[46,47]

Preparation of curcumin-based Pt(II) complexes and cell lines

Stock solutions of curcumin-based Pt(II) complexes **1–5** in dimethyl sulfoxide (DMSO, Sigma-Aldrich, USA) were prepared at a concentration of 10 mg ml^{-1}. Working solutions were freshly prepared according to the experimental design by serial dilutions in a complete culture medium. The *in vitro* activity of the molecules was tested against the following human cell lines: triple-negative breast cancer (MDA-MB 231),[48]

osteosarcoma (SK-ES1), melanoma (M20), and dermal fibroblasts (hSDFs).[49]

Cell lines were maintained by 1:10 and 1:20 weekly dilutions in Dulbecco's Modified Eagle Medium (DMEM LG) (MDA-MB 231 and SK-ES1), Iscove's Modified Dulbecco's Medium (IMDM) (M20), and Eagle's Minimum Essential Medium (EMEM) (hSDFs), supplemented with 10% Foetal Bovine Serum (FBS). All reagents for cell culture were provided by Euroclone, UK.

In vitro sensitivity of cell lines to curcumin-based Pt(II) complexes

The effect of **3**, **4** and **5** against cell proliferation or cell viability has been evaluated in 96 multiwell plates (Euroclone, UK). Briefly, 1:2 serial dilutions of pure molecules (from 0.54 to 140 μM) were prepared in 100 μl of culture medium per well and then 2000 tumour cells were added to each well. After 7 d of culture (antiproliferative assay) at 37 °C and 5% CO_2, cell growth was evaluated by the MTT assay (3-(4,5-dimethyl-2-thiazolyl)-2,5-diphenyl-2-*H*-tetrazolium) as previously described.[50,51] The cytotoxicity assay (24 h at 37 °C, 5% CO_2) was performed at increasing concentrations (from 8 to 140 μM) with 10 000 cells per well. The inhibitory concentration (IC_{50}) was determined according to the Reed & Muench formula using Excel (Microsoft, Inc, Albuquerque, NM, USA).[52,53] The stability of the molecules was evaluated by incubation at 37 °C with 5% CO_2 in the complete cell culture medium for 24, 48, 72 and 96 hours, then the molecules were tested using the anti-proliferative assay, and IC_{50} values were compared with those obtained with fresh molecules.

Statistical analysis

Data are expressed as average ± standard deviation (SD). Differences between mean values were evaluated according to Student's *t*-test performed using the GRAPHPADINSTAT program (GraphPad Software Inc., San Diego, CA, USA). *p*-Values ≤ 0.05 were considered statistically significant. The linearity of response and the correlation were studied using regression analysis using Excel 2013 software (Microsoft, Inc., Albuquerque, New Mexico, USA).[54]

Results and discussion

Synthesis and characterization of [(C^N)Pt(curc)] complexes, 1–5

For this study, the selected H(C^N) cyclometallating ligands were H(ppy) referring to 2-phenylpyridine, H(ppy-F) 2-(2,4-difluorophenyl)pyridine, H(Bzq) benzo[*h*]quinoline, and H(tpy) 2-(2-thienyl)pyridine and H(pq) referring to 2-phenylquinoline. These ligands coordinate to the Pt(II) center forming stable five-membered chelate rings. The DMSO (dimethyl sulfoxide) and chloride ligands in the mononuclear precursors or only the bridging chloride ligands in the case of the binuclear precursors occupy the remaining coordination sites in a square planar geometry typical of Pt(II) complexes. The novel **[(C^N)Pt**

(curc)] complexes, **1**–**5**, were easily synthesized through a microwave assisted procedure by reacting previously reported precursors **[(C^N)Pt(DMSO)(Cl)]** or **[(C^N)Pt(H(C^N))(Cl)]**[41–43] with a slight excess of H(curc) and triethylamine (NEt₃) (Scheme 1); note that the synthesis and characterization of the novel precursor **[(pq)Pt(DMSO)(Cl)]** complex, **V**, are reported in the ESI.† Remarkably, in addition to the significantly shortened reaction time, due to the microwave irradiation, it is worth emphasizing that the use of NEt₃ as a base introduces an important advantage in comparison with the synthetic method currently present in the literature, in which the thallium salt of curcumin is usually employed for the synthesis of curc–metal complexes.[55] These complexes were obtained as orange or yellow powders with high yields, reaching up to 80%. The isolated products have been fully characterized (melting point, elemental analysis, FT-IR, NMR and MS spectroscopy), are stable in air and exhibit low solubility in most common organic solvents, with the exception of DMSO. The FT-IR spectra of complexes **1**–**5** (see the ESI, Fig. S1†), proved the curc–ligand coordination by the shift of bands predominantly related to overlapping stretching vibrations of (C=C) and (C=O) of curc. Indeed, while in the free ligand, H(curc), these two bands are found at 1628 cm⁻¹ and 1603 cm⁻¹, in the IR spectra of the complexes, they slightly shift to lower wavenumbers, in the ranges 1625–1622 cm⁻¹ and 1607–1591 cm⁻¹, respectively. In the ¹H-NMR spectra of the Pt(II) complexes, the characteristic signals of the proton (Hᵃ) of the methylene group and the methoxy groups of the coordinated curc are shifted to higher
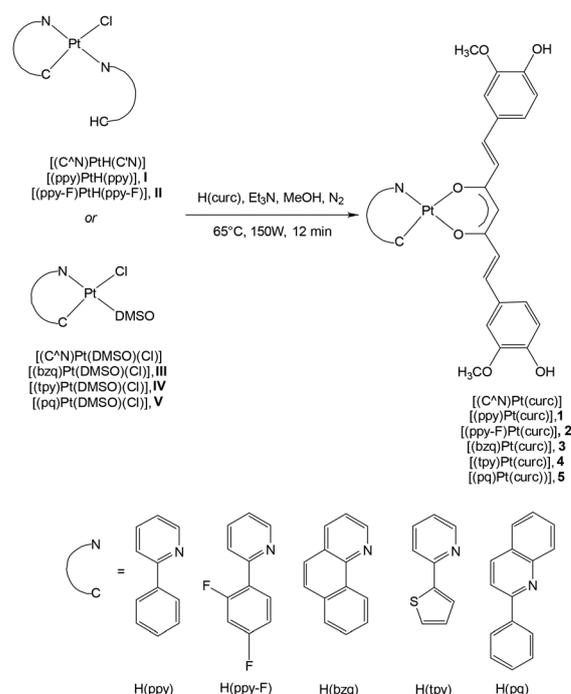
Scheme 1 Synthesis of complexes **1–5**, reagents and conditions (H(ppy), 2-phenylpyridine, H(ppy-F), 2-(2,4-difluorophenyl)pyridine, H(Bzq), benzo-[*h*]quinoline, H(tpy), 2-(2-thienyl)pyridine and H(pq), 2-phenylquinoline).

fields with respect to those of H(curc), also confirming the metal–ligand coordination.[35] All spectra, recorded in DMSO-d$_6$, have shown the signal of the H^a methylene proton in the range 5.95–6.05 ppm with variation with respect to H(curc), analogously to that reported in the literature.[55] Other confirmations of the synthetic protocol are related to modifications of signals of protons of cyclometalated ligands. In particular, this is supported by the shift toward the lower field of the proton in the α position with respect to the N-coordinated atom, thus confirming the formation of desired complexes.[41] All ^{1}H-NMR, ^{13}C-NMR and ESI-MS spectra of the new complexes **1–5** are presented in the ESI (Fig. S2–S6†).

Lipophilicity

Lipophilicity was evaluated for assessing the ability of the [(C^N)Pt(curc)] complexes to satisfy drug-likeness criteria (see Table S1†). All the complexes complied with Lipinski's rule associated with a high MW, with log P values ranging from 3.15 to 3.76, comparable to the value of log P for H(curc) reported in the literature.[56] These log P values underlined the ability of the [(C^N)Pt(curc)] complexes **1–5** to well permeate and be taken up through the cell lipid bilayer membrane to reach the site of action.[47]

Photophysical characterization

The photophysical characterization of **1–5** and H(curc) was carried out in DMSO diluted solutions. All solutions showed a pale-yellow colour at the investigated concentrations and their absorption spectra are reported in Fig. 1.

The H(curc) absorption spectrum (Fig. 1, black line) shows a broad and intense absorption band in the visible region of the electromagnetic spectrum with the maximum centred at 435 nm, attributed to the π–π* transitions of its enolic form. The presence of a shoulder at 455 nm is probably due to the presence of the isomeric form in the ground state.[57–59]

For a better description of the spectral features of **1–5**, the two distinct regions in the absorption spectra, i.e., the visible

and the UV region, will be separately considered. In the visible region, the shape of the spectra is quite similar for all complexes, so the main features will be discussed together. This is due to the presence of curc-Pt electronic transitions that generate a large double-peaked band with maxima at around 470 and 440 nm and a shoulder centred at 420 nm. The red shifted peak and the 420 nm shoulder are both attributed to the ligand-to-metal charge transfer (LMCT) transition from curc to the metal centre, while the blue shifted peak is due to a π–π* ligand centred (LC) transition on curc. The latter is red shifted with respect to the analogous transition in H(curc) due to the coordination with the Pt centre.[25,60,61] The only differences observed in the visible region involve negligible variations in the position of the aforementioned band and a different interband ratio for **2** compared with **1**, attributable to the presence of the strong electronegative fluorine atom in the molecular structure. In the UV region, the spectra show marked differences due to the electronic transitions localized on the different (C^N) ligands.

The emission spectra of H(curc) and **1–5** are reported in Fig. 2, while the main data are reported in Table 1. H(curc) shows a large and de-structured fluorescence band centred at 550 nm with an emission lifetime equal to 0.3 ns. **1–5** show a similar photophysical behaviour also in emission, that is almost identical to that of H(curc). An emission band centred around 545 nm with a shoulder around 610 nm was detected. The presence of this double peaked emission is attributable to the greater structural rigidity of the complexes than the free ligand, conferred by the presence of the metal centre. The decay from the excited states shows in these cases bi-exponential kinetics with a short lifetime of 0.3 ns and a longer one of almost 7 ns (only for **3** was measured a longer lifetime of 12.8 ns). Based on these data, the detected emissions can be attributed to the contemporary presence in solution of two different emissive species: H(curc) responsible for the shorter lifetime and the corresponding Pt complexes with longer decay times. The contribution to the signal of H(curc) is approximately
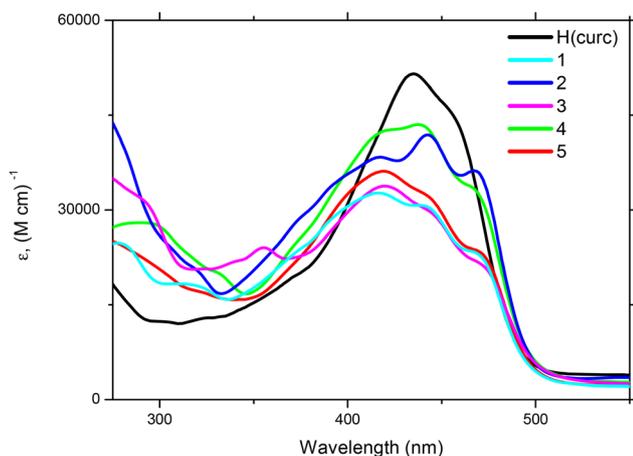

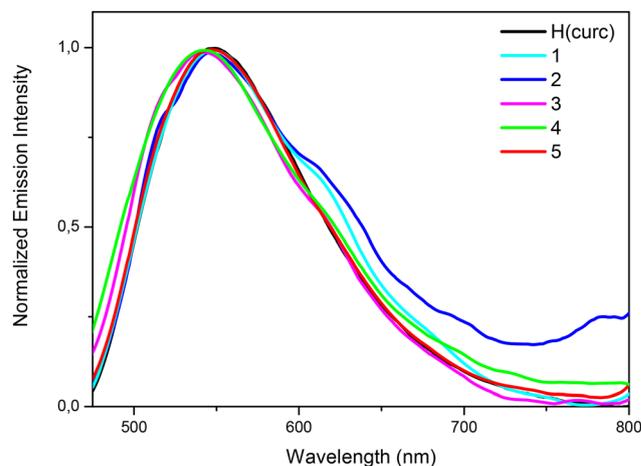**Fig. 1** Absorption spectra of **H(curc)** and **1–5** in DMSO diluted solutions.

Fig. 2 Emission spectra of **H(curc)** and **1–5** in DMSO diluted solutions.

Table 1 Main photophysical data of **H(curc)** and complexes **1–5**

Compound	Absorption maxima (nm) [molar absorptivity, ε (M cm)$^{-1}$]	Emission maximum λ_{em} (nm)	Lifetime, τ (ns) [weight] (%)	
H(curc)	455 [45 600], 435 [51 600]	550	0.3	
1	468 [23 300], 441 [30 700], 420 [32 700], 310 [18 400], 280 [24 700]	545, 610	6.8 [25]	0.3 [75]
2	468 [36 300], 443 [42 100], 417 [38 500], 320 [20 700], 305 [24 100]	545, 617	12.8 [23]	0.3 [77]
3	467 [23 800], 440 [32 600], 420 [36 100]	540, 610	7.5 [23]	0.3 [77]
4	466 [33 700], 439 [43 500], 420 [42 600], 330 [20 100], 295 [27 800]	540, 615	7.1 [18]	0.3 [82]
5	470 [21 600], 440 [30 400], 420 [33 800], 355 [34 300], 338 [21 800], 290 [31 800]	545, 620	7.1 [12]	0.3 [78]

three times more relevant, probably because the emission quantum yield of H(curc) is greater than that of the corresponding Pt complexes, as already observed for other Pt(II)–curc complexes.[7,62] Furthermore, by recording the emission spectra at increasing time intervals, an increase in the emission intensity was observed for all the samples (see the ESI, Fig. S7–S11†). The extinction spectra collected for these emission signals match that of H(curc) (see the ESI, Fig. S12†), suggesting the release of the ligand with time. The confirmation of this behaviour was obtained by observing the photophysical properties of sample **1** in the solid state (only the powders of **1** are emissive in the solid state) and in a different solvent, *i.e.*, CH$_2$Cl$_2$.

In the solid state, an emission band that shows two different maxima, *i.e.*, 605 and 655 nm, was detected (see Fig. 3). These data compared with emission and excitation spectra of H(curc) in the solid state suggest that in the solid state only the complex is present, as confirmed by the photophysical characterization of **1** in CH$_2$Cl$_2$ diluted solution (see the ESI, Fig. S13†). In this solvent, the sample is not emissive, but after 30 and 60 minutes an emission coherent with that of H(curc) was detected (see the ESI, Fig. S14†). Thus, we can conclude that in solution, **1–5** experienced a slow release of H(curc), a phenomenon already observed in the literature for similar samples, but in that case induced by strong irradiation with UV light.[7,8] This phenomenon was observed only by emission spectroscopy, due to the higher sensitivity of the technique, so we can speculate that the release of H(curc) is very limited in quantity and will not compromise the exploitation of the complexes as anticancer agents. To evaluate the stability of the complexes under the conditions in which the biological tests were performed, 10 mg of each complex were dissolved in 1 mL of DMSO, before being diluted in a ratio of 1/100 in aqueous PBS buffer solution. The absorption spectra of these solutions were collected after 0, 20, 24, 44, 48, 68 and 72 h of preparation (see the ESI, Fig. S15†). In no case a significant change was observed in the shape of the spectrum, thus indicating that the complexes are stable under the experimental conditions. The changes, where observed, consisted of an increase or decrease in the intensity of the absorption over time, attributed to the solubility of the complexes. To analyse the results, absorbance values (measured at the most significant peak for each complex) were plotted against time and least squares lines were plotted to account for any inaccuracies (see the ESI, Fig. S16†). While complexes **1** and **5** show constant absorption spectra in the time range explored, indicating complete solubilization, complex **3** shows an absorption spectrum whose intensity increases over time, probably due to slow solubilization. Finally, complexes **2** and **4** show absorption spectra whose intensity decreases, suggesting that slight precipitation occurs over time.

In vitro anticancer activity of complexes 1–5

The antiproliferative activity was evaluated on human fibroblast (hSDF) proliferation (Fig. 4).

Given the stronger antiproliferative effects exhibited by complexes **3**, **4**, and **5**, we decided to further investigate their potential against different types of cancer cell lines including triple-negative breast cancer (MDA-MB 231), human Ewing's sarcoma (SK-ES1) and melanoma (M20). These cell lines were selected because they exemplify three very different cancer types, each with distinct biological and molecular characteristics. In particular, MDA-MB-231 is an aggressive and highly invasive breast cancer cell line, lacking expression of estrogen receptor (ER), progesterone receptor (PR), and HER2 and it is often used in studies of drug resistance, metastasis, and epithelial–mesenchymal transition (EMT). SK-ES1 is a bone cancer cell line derived from Ewing's sarcoma, a highly aggressive and metastatic tumor typically affecting children and young adults, often used to study tumorigenic mechanisms of sarcomas and their response to chemotherapy. M20 is a skin
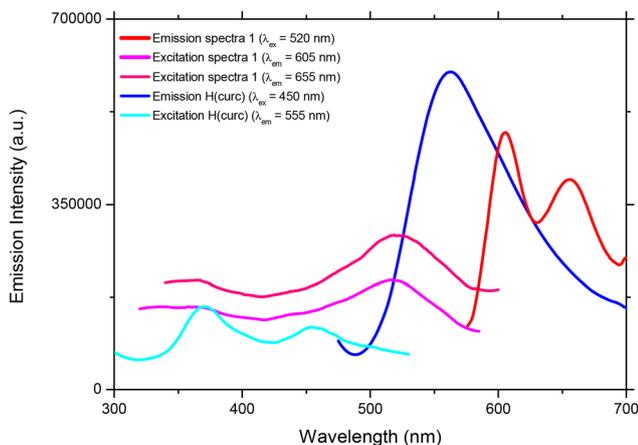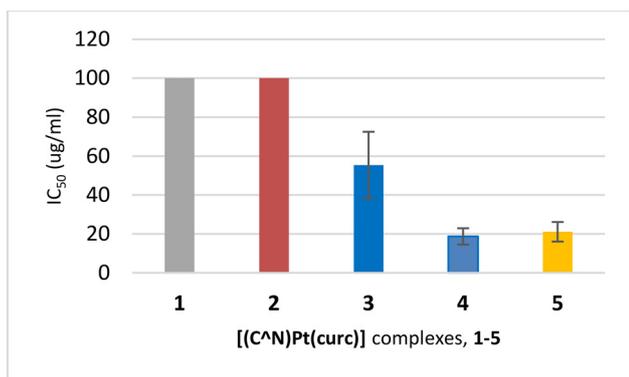

Fig. 3 Emission and excitation spectra of **1** and **H(curc)** powder.

Fig. 4 Antiproliferative activity on human fibroblasts (hSDFs). Columns represent the mean of IC_{50} values from at least three experiments. Error bars represent the Standard Error of the Mean (SEM).

cancer cell line, highly metastatic, and used to study immune evasion and targeted therapies.

For these peculiar features, drug response differences were verified in terms of antiproliferative activity, considering the limited success of the commonly used chemotherapeutics toward these aggressive cancer phenotypes and considering the adjuvant role of **H(curc)** in cancer therapies.[63–65]

As reported in Table 2, the drugs showed antiproliferative activity against all the cancer cell lines tested. The sarcoma cells (SK-ES1) were found to be more responsive to the selected **[(C^N)Pt(curc)]** complexes, showing a significantly higher sensitivity ($p < 0.02$) to **4** and **5**, with IC_{50} values of 15.42 + 1.01 μM and 13.91 ± 0.16 μM, respectively. Complex **3**, conversely, exhibited lower activity against M20 and SK-ES1 cells, although still modest (21.29 ± 3.2 μM and 33.41 ± 3.3 μM), and dramatically lower activity against MDA-MB 231 cancer cells (88.77 ± 5.5 μM).

The two more active complexes **4** and **5** were also tested for their cytotoxicity at 24 h (Table 3), which was found to be expressed at a quite different level in the cancer cell lines: complex **4** was relatively less toxic than **5** towards MDA-MB 231 and SK-ES1, while showing comparable activity to that of complex **5** against M20. Complex **5** proves to be the most cyto-

Table 3 *In vitro* cytotoxic activity of **4** and **5** on three cancer cell lines: triple-negative breast cancer (MDA-MB 231), melanoma (M20), and osteosarcoma (SK-ES1). Data are expressed as the percentage of cell growth normalized on control cells. The table reports the mean of IC50 values (μM) ± Standard Deviation (SD) for each tested compound and each cell line

Compound	MDA-MB 231 IC_{50} values (μM)	SK-ES1 IC_{50} values (μM)	M20 IC_{50} values (μM)
4	>138.3	>138.3	30.46 ± 0.4
5	78.61 ± 3.71	26.11 ± 1.99	39.18 ± 4.04

toxic complex, although to a significantly lesser extent against MDA-MB 231.

Finally, the antiproliferative activity of the two most active complexes, **4** (Fig. 5A) and **5** (Fig. 5B), was evaluated after 24, 48, 72 and 96 h of incubation at 37 °C. As a general behaviour, the antitumor activity decreases over time with some differences depending on the target cell line. Both complexes **4** and **5** retain their full activity towards SK-ES1 and M20 for up to 72 h of treatment, but their activity is reduced by half after 96 hours of treatment. Surprisingly, a different behaviour can be observed when taking into consideration the MDA-MB 231 cell line, in which the activity drops to half after just 48 hours of treatment. The *in vitro* experiments confirm the 72 h stability of these complexes, as previously demonstrated by the spectroscopic studies.
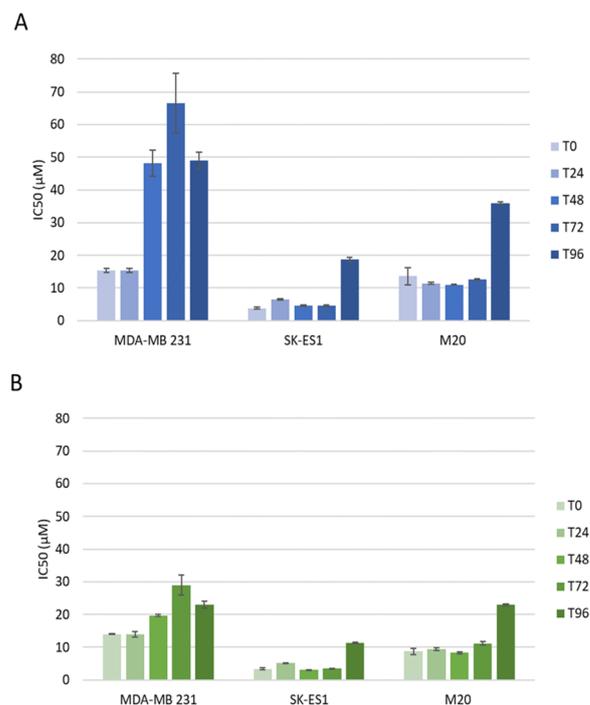
Fig. 5 Antiproliferative activity of (A) complex **4** and (B) complex **5** upon incubation in cell media at 37 °C for 0, 24, 48, 72 and 96 hours. Antiproliferative activity was evaluated on triple-negative breast cancer (MDA-MB 231), osteosarcoma (SK-ES1) and melanoma (M20) cell lines. Columns represent the mean of IC50 values from at least three experiments. Error bars represent the Standard Error of the Mean (SEM).

Table 2 *In vitro* antiproliferative activity of **3**, **4**, and **5** on three cancer cell lines: triple-negative breast cancer (MDA-MB 231), osteosarcoma (SK-ES1) and melanoma (M20). Data are expressed as the percentage of cell growth normalized on untreated control cells, and the bars represent the Standard Error of the Mean (SEM). The table reports the mean of IC_{50} values (μM) ± Standard Deviation (SD) for each tested compound and each cell line

| Compound	MDA-MB 231 IC_{50} values (μM)	SK-ES1 IC_{50} values (μM)	M20 IC_{50} values (μM)
Cisplatin	59.4 ± 2.3	1.82 ± 0.87	18.73 ± 6.23
3	88.77 ± 5.5	21.29 ± 3.2	33.41 ± 3.3
4	15.42 ± 1.01	3.8 ± 0.86	13.59 ± 7.88
5	13.91 ± 0.16	3.41 ± 0.99	8.72 ± 2.6

Conclusions

The [(C^N)Pt(curc)] complexes, **1–5**, investigated in this study exhibited significant antiproliferative activity, with complexes **3–5** in general exhibiting a more significant antitumor effect on the sarcoma cell line SK-E21. Notably, this effect was observed in the absence of photoactivation, a feature commonly required for curcumin-containing compounds to exert their biological activity. This could explain, at least in part, also the marked sensitivity of healthy fibroblasts to the complexes. Some discrepancy between the antiproliferative and cytotoxic activity, revealed especially for compounds **4** and **5**, may be related to the differences in the mechanism of action of the drugs considered, which may differentially affect the balance between cell killing and cell cycle arrest mechanisms. This apparent divergence could be even amplified by the structural features of the complex and/or the biological features of the cancer cell line considered, likely related to differences in DNA repair abilities. Both complexes **4** and **5** express their full activity towards SK-ES1 and M20 for up to 72 h of treatment, but their activity halves after 96 hours of treatment, in accordance with the stability investigation by spectroscopic studies. Surprisingly, the behaviour is different when referring to MDA-MB 231, in which the activity is reduced by half after just 48 h of treatment, showing a better ability of such cancer cells to restore their functionality and allowing them to overcome the cytotoxicity of the complexes within a shorter time frame. Recognizing that photoactivation is not necessary for this series of curcumin-based Pt(II) complexes, their relative stability in solution and the preliminary results in terms of antiproliferative activity toward SK-ES1 make complexes **4** and **5** promising candidates for the treatment of Ewing's sarcoma.

Conflicts of interest

There are no conflicts to declare.

Data availability

The datasets supporting this article have been uploaded as part of the ESI.† Additional data can be provided upon reasonable request to the authors.

Acknowledgements

References

1 J. Kuzminska, P. Szyk, D. T. Mlynarczyk, P. Bakun, I. Muszalska-Kolos, K. Dettlaff, A. Sobczak, T. Goslinski and A. Jelinska, Curcumin Derivatives in Medicinal Chemistry: Potential Applications in Cancer Treatment, *Molecules*, 2024, **29**, 5321.

2 K. Kaur, A. K. Al-Khazaleh, D. J. Bhuyan, F. Li and C. G. Li, A Review of Recent Curcumin Analogues and Their Antioxidant, Anti-Inflammatory, and Anticancer Activities, *Antioxidants*, 2024, **13**, 1092.

3 A. Adlia, C. C. Aslan, L. Safitri and I. K. Adnyana, Turmeric-black pepper-honey nanoemulsion formulation and antiulcerogenic effect evaluation against ethanol-induced gastric ulcers in rats, *PLoS One*, 2025, **20**, e0317899.

4 Q. Sun, Q. Niu, Y. Guo, Y. Zhuang, X. Li, J. Liu, N. Li, Z. Li, F. Huang and Z. Qiu, Regulation on Citrate Influx and Metabolism through Inhibiting SLC13A5 and ACLY: A Novel Mechanism Mediating the Therapeutic Effects of Curcumin on NAFLD, *J. Agric. Food Chem.*, 2021, **69**, 8714–8725.

5 N. Azari Torbat, I. Akbarzadeh, N. Rezaei, Z. Salehi Moghaddam, S. Bazzazan and E. Mostafavi, Curcumin-Incorporated Biomaterials: In silico and in vitro evaluation of biological potentials, *Coord. Chem. Rev.*, 2023, **492**, 215233.

6 L. Z. Racz, C. P. Racz, L. C. Pop, G. Tomoaia, A. Mocanu, I. Barbu, M. Sárközi, I. Roman, A. Avram, M. Tomoaia-Cotisel and V. A. Toma, Strategies for Improving Bioavailability, Bioactivity, and Physical-Chemical Behavior of Curcumin, *Molecules*, 2022, **27**, 6854.

7 B. Laha, A. R. Tiwari, E. Gravel, E. Doris and I. N. N. Namboothiri, The Michael donor–acceptor reactivity of curcumins in the synthesis of diverse multi-functional scaffolds, *Org. Biomol. Chem.*, 2024, **22**, 1346–1359.

8 M. Salem, S. Rohani and E. R. Gillies, Curcumin, a promising anti-cancer therapeutic: a review of its chemical properties, bioactivity and approaches to cancer cell delivery, *RSC Adv.*, 2014, **4**, 10815–10829.

9 L. Shen and H.-F. Ji, The pharmacology of curcumin: is it the degradation products?, *Trends Mol. Med.*, 2012, **18**, 138–144.

10 Y. Chen, C. Chen, X. Zhang, C. He, P. Zhao, M. Li, T. Fan, R. Yan, Y. Lu, R. J. Lee, M. W. Khan, M. Sarfraz, X. Ma, T. Yang and G. Xiang, Platinum complexes of curcumin delivered by dual-responsive polymeric nanoparticles improve chemotherapeutic efficacy based on the enhanced anti-metastasis activity and reduce side effects, *Acta Pharm. Sin. B*, 2020, **10**, 1106–1121.

11 M. S. Refat, Synthesis and characterization of ligational behavior of curcumin drug towards some transition metal ions: Chelation effect on their thermal stability and biological activity, *Spectrochim. Acta, Part A*, 2013, **105**, 326–337.

12 S. Banerjee and A. R. Chakravarty, Metal Complexes of Curcumin for Cellular Imaging, Targeting, and

Photoinduced Anticancer Activity, *Acc. Chem. Res.*, 2015, **48**, 2075–2083.

13 L. Zeng, P. Gupta, Y. Chen, E. Wang, L. Ji, H. Chao and Z. S. Chen, The development of anticancer ruthenium(ii) complexes: from single molecule compounds to nanomaterials, *Chem. Soc. Rev.*, 2017, **46**, 5771–5804.

14 S. Prasad, D. DuBourdieu, A. Srivastava, P. Kumar and R. Lall, Metal-Curcumin Complexes in Therapeutics: An Approach to Enhance Pharmacological Effects of Curcumin, *Int. J. Mol. Sci.*, 2021, **22**, 7094.

15 B. Zebib, Z. Mouloungui and V. Noirot, Stabilization of Curcumin by Complexation with Divalent Cations in Glycerol/ Water System, *Bioinorg. Chem. Appl.*, 2010, **2010**, 292760.

16 N. Saewan, A. Thakam, A. Jintaisong and K. Kittigowittana, Anti-tyrosinase and cytotoxicity activities of curcumin-metal complexes, *Int. J. Pharm. Pharm. Sci.*, 2014, **6**, 270–273.

17 Z. Fu, X. Chen, S. Guan, Y. Yan, H. Lin and Z.-C. Hua, Curcumin inhibits angiogenesis and improves defective hematopoiesis induced by tumor-derived VEGF in tumor model through modulating VEGF-VEGFR2 signaling pathway, *Oncotarget*, 2015, **6**, 19469.

18 R. Mondal, M. Keerthana, N. Pandurangan and S. Shanmugaraju, Zn(II)-Curcumin Complexes-Based Anticancer Agents, *ChemMedChem*, 2024, **19**, e202400558.

19 F. E. Jacinto, L. P. de Oliveira, A. A. Batista, K. M. Oliveira and R. S. Correa, Ruthenium(II) complexes of curcumin and β-diketone derivatives: effect of structural modifications on their cytotoxicity, *R. Soc. Open Sci.*, 2024, **11**, 240353.

20 M. Ghosh and N. Sarkar, Exploring the World of Curcumin: Photophysics, Photochemistry, and Applications in Nanoscience and Biology, *ChemBioChem*, 2024, **25**, e202400335.

21 S. Mondal, S. Ghosh and S. P. Moulik, Stability of curcumin in different solvent and solution media: UV–visible and steady-state fluorescence spectral study, *J. Photochem. Photobiol., B*, 2016, **158**, 212–218.

22 A. Wolnicka-Glubisz and A. Wisniewska-Becker, Dual Action of Curcumin as an Anti- and Pro-Oxidant from a Biophysical Perspective, *Antioxidants*, 2023, **12**, 1725.

23 T. A. Dahll, P. Bilski, K. J. Reszka and C. F. Chignell, PHOTOCYTOTOXICITY OF CURCUMIN, *Photochem. Photobiol.*, 1994, **59**, 290–294.

24 N. Mukherjee, A. Raghavan, S. Podder, S. Majumdar, A. Kumar, D. Nandi and A. R. Chakravarty, Photocytotoxic Activity of Copper(II) and Zinc(II) Complexes of Curcumin and (Acridinyl)dipyridophenazine, *ChemistrySelect*, 2019, **4**, 9647–9658.

25 K. Mitra, S. Gautam, P. Kondaiah and A. R. Chakravarty, The cis-Diammineplatinum(II) Complex of Curcumin: A Dual Action DNA Crosslinking and Photochemotherapeutic Agent, *Angew. Chem., Int. Ed.*, 2015, **54**, 13989–13993.

26 R. Kushwaha, V. Singh, S. Peters, A. K. Yadav, D. Dolui, S. Saha, S. Sarkar, A. Dutta, B. Koch, T. Sadhukhan and S. Banerjee, Density Functional Theory-Guided Photo-

27 B. Zhang, J. a. Xiao, X. Wang, P. Li and W. Su, Synthesis, characterization and photodynamic activity of half-sandwich rhodium(III) complexes with curcuminoids, *Photodiagn. Photodyn. Ther.*, 2020, **32**, 102049.

28 A. Jana, S. Sahoo, S. Paul, S. Sahoo, C. Jayabaskaran and A. R. Chakravarty, Photodynamic Therapy with Targeted Release of Boron-Dipyrromethene Dye from Cobalt(III) Prodrugs in Red Light, *Inorg. Chem.*, 2024, **63**, 6822–6835.

29 S. Prasad, D. DuBourdieu, A. Srivastava, P. Kumar and R. Lall, Metal–Curcumin Complexes in Therapeutics: An Approach to Enhance Pharmacological Effects of Curcumin, *Int. J. Mol. Sci.*, 2021, **22**, 7094.

30 B. M. de França, S. S. C. Oliveira, L. O. P. Souza, T. P. Mello, A. L. S. Santos and J. S. Bello Forero, Synthesis and photophysical properties of metal complexes of curcumin dyes: Solvatochromism, acidochromism, and photoactivity, *Dyes Pigm.*, 2022, **198**, 110011.

31 X. Tian, Y. Zhu, M. Zhang, L. Luo, J. Wu, H. Zhou, L. Guan, G. Battaglia and Y. Tian, Localization matters: a nuclear targeting two-photon absorption iridium complex in photodynamic therapy, *Chem. Commun.*, 2017, **53**, 3303–3306.

32 G. De Soricellis, F. Fagnani, A. Colombo, C. Dragonetti and D. Roberto, Exploring the potential of N^C^N cyclometalated Pt(II) complexes bearing 1,3-di(2-pyridyl)benzene derivatives for imaging and photodynamic therapy, *Inorg. Chim. Acta*, 2022, **541**, 121082.

33 M. Fereidoonnezhad, B. Kaboudin, T. Mirzaee, R. Babadi Aghakhanpour, M. Golbon Haghighi, Z. Faghih, Z. Faghih, Z. Ahmadipour, B. Notash and H. R. Shahsavari, Cyclometalated Platinum(II) Complexes Bearing Bidentate O,O′-Di(alkyl)dithiophosphate Ligands: Photoluminescence and Cytotoxic Properties, *Organometallics*, 2017, **36**, 1707–1717.

34 K. Aysola, A. Desai, C. Welch, J. Xu, Y. Qin, V. Reddy, R. Matthews, C. Owens, J. Okoli, D. J. Beech, C. J. Piyathilake, S. P. Reddy and V. N. Rao, Triple Negative Breast Cancer - An Overview, *Hered. Genet.*, 2013, (Suppl 2), 001.

35 P. Zagami and L. A. Carey, Triple negative breast cancer: Pitfalls and progress, *npj Breast Cancer*, 2022, **8**, 95.

36 A. Misaghi, A. Goldin, M. Awad and A. A. Kulidjian, Osteosarcoma: a comprehensive review, *Soc. J.*, 2018, **4**, 12.

37 G. M. Robbins, Y. Y. Vue, E. P. Rahrmann and B. S. Moriarity, Osteosarcoma: A comprehensive review of model systems and experimental therapies, *Med. Res. Arch.*, 2024, **12**, 6000.

38 M.-y. Hsieh, S.-K. Hsu, T.-Y. Liu, C.-Y. Wu and C.-C. Chiu, Melanoma biology and treatment: a review of novel regulated cell death-based approaches, *Cancer Cell Int.*, 2024, **24**, 63.

39 G. Coffetti, M. Moraschi, G. Facchetti and I. Rimoldi, The Challenging Treatment of Cisplatin-Resistant Tumors: State of the Art and Future Perspectives, *Molecules*, 2023, **28**, 3407.

40 I. Rimoldi, V. Coccè, G. Facchetti, G. Alessandri, A. T. Brini, F. Sisto, E. Parati, L. Cavicchini, G. Lucchini, F. Petrella, E. Ciusani and A. Pessina, Uptake-release by MSCs of a cationic platinum(II) complex active in vitro on human malignant cancer cell lines, Biomed. Pharmacother., 2018, 108, 111–118.

41 N. Godbert, T. Pugliese, I. Aiello, A. Bellusci, A. Crispini and M. Ghedini, Efficient, Ultrafast, Microwave-Assisted Syntheses of Cycloplatinated Complexes, Eur. J. Inorg. Chem., 2007, 2007, 5105–5111.

42 A. Ionescu, N. Godbert, I. Aiello, L. Ricciardi, M. La Deda, A. Crispini, E. Sicilia and M. Ghedini, Anionic cyclometalated Pt(ii) and Pt(iv) complexes respectively bearing one or two 1,2-benzenedithiolate ligands, Dalton Trans., 2018, 47, 11645–11657.

43 A. Ionescu, R. Lento, T. F. Mastropietro, I. Aiello, R. Termine, A. Golemme, M. Ghedini, N. Bellec, E. Pini, I. Rimoldi and N. Godbert, Electropolymerized Highly Photoconductive Thin Films of Cyclopalladated and Cycloplatinated Complexes, ACS Appl. Mater. Interfaces, 2015, 7, 4019–4028.

44 G. Palermo, D. Pagnotto, L. Ricciardi, L. Pezzi, M. La Deda and A. De Luca, Thermoplasmonic Effects in Gain-Assisted Nanoparticle Solutions, J. Phys. Chem. C, 2017, 121, 24185–24191.

45 A. Crispini, D. Pucci, I. Aiello and M. Ghedini, Synthesis and crystal structure of dinuclear cyclopalladated 1,2- and 1,3-bridged squarato complexes, Inorg. Chim. Acta, 2000, 304, 219–223.

46 G. Mazzone, S. Scoditti, R. Caligiuri, L. Ricciardi, E. Sicilia, M. G. Lupo, I. Rimoldi, N. Godbert, M. La Deda, A. Ionescu, M. Ghedini, I. Aiello and G. Facchetti, Cytotoxicity of Alizarine versus Tetrabromocathecol Cyclometalated Pt(II) Theranostic Agents:A Combined Experimental and Computational Investigation, Inorg. Chem., 2022, 61, 7188.

47 R. Caligiuri, G. Di Maio, N. Godbert, F. Scarpelli, A. Candreva, I. Rimoldi, G. Facchetti, M. G. Lupo, E. Sicilia, G. Mazzone, F. Ponte, I. Romeo, M. La Deda, A. Crispini, R. De Rose and I. Aiello, Curcumin-based ionic Pt(ii) complexes: antioxidant and antimicrobial activity, Dalton Trans., 2022, 51, 16545–16556.

48 R. Cailleau, M. Olivé and Q. V. J. Cruciger, Long-term human breast carcinoma cell lines of metastatic origin: Preliminary characterization, In Vitro, 1978, 14, 911–915.

49 P. Mesdom, R. Colle, E. Lebigot, S. Trabado, E. Deflesselle, B. Fève, L. Becquemont, E. Corruble and C. Verstuyft, Human Dermal Fibroblast: A Promising Cellular Model to Study Biological Mechanisms of Major Depression and Antidepressant Drug Response, Curr. Neuropharmacol., 2020, 18, 301–318.

50 V. Coccè, A. Vitale, S. Colombo, A. Bonomi, F. Sisto, E. Ciusani, G. Alessandri, E. Parati, P. Brambilla, M. Brambilla, C. A. La Porta and A. Pessina, Human skin–derived fibroblasts used as a 'Trojan horse' for drug delivery, Clin. Exp. Dermatol., 2016, 41, 417–424.

51 A. Pessina, A. Bonomi, V. Coccè, G. Invernici, S. Navone and L. Cavicchini, Mesenchymal stromal cells primed with paclitaxel provide a new approach for cancer therapy, PLoS One, 2011, 6, e28321.

52 T. Mosmann, Rapid colorimetric assay for cellular growth and survival: Application to proliferation and cytotoxicity assays, J. Immunol. Methods, 1983, 65, 55–63.

53 L. J. Reed and H. Muench, A simple method of estimating fifty per cent endpoints, Am. J. Epidemiol., 1938, 27, 493–497.

54 E. Corsini, G. Facchetti, S. Esposito, A. Maddalon, I. Rimoldi and M. S. Christodoulou, Antiproliferative effects of chalcones on T cell acute lymphoblastic leukemia-derived cells: Role of PKCβ, Arch. Pharm., 2020, e2000062, DOI: 10.1002/ardp.202000062.

55 M. K. Raza, K. Mitra, A. Shettar, U. Basu, P. Kondaiah and A. R. Chakravarty, Photoactive platinum(ii) β-diketonates as dual action anticancer agents, Dalton Trans., 2016, 45, 13234–13243.

56 R. Tabanelli, S. Brogi and V. Calderone, Improving Curcumin Bioavailability: Current Strategies and Future Perspectives, Pharmaceutics, 2021, 13, 1715.

57 A. Balaban, C. Párkányi, I. Ghiviriga, J.-J. Aaron, Z. Zajickova and O. Martinez, Curcumin–Benzodioxaborole Chelates, Arkivoc, 2008, 13, 1–9.

58 U. S. Raikar, C. G. Renuka, Y. F. Nadaf, B. G. Mulimani, A. M. Karguppikar and M. K. Soudagar, Solvent effects on the absorption and fluorescence spectra of coumarins 6 and 7 molecules: Determination of ground and excited state dipole moment, Spectrochim. Acta, Part B, 2006, 65, 673–677.

59 K. I. Priyadarsini, Photophysics, photochemistry and photobiology of curcumin: Studies from organic solutions, bio-mimetics and living cells, J. Photochem. Photobiol., C, 2009, 10, 81–95.

60 A. Upadhyay, S. Gautam, V. Ramu, P. Kondaiah and A. R. Chakravarty, Photocytotoxic cancer cell-targeting platinum(ii) complexes of glucose-appended curcumin and biotinylated 1,10-phenanthroline, Dalton Trans., 2019, 48, 17556–17565.

61 K. Mitra, S. Gautam, P. Kondaiah and A. R. Chakravarty, Platinum(II) Complexes of Curcumin Showing Photocytotoxicity in Visible Light, Eur. J. Inorg. Chem., 2017, 2017, 1753–1763.

62 C. Párkányi, A. M. Shafik, A. Jean-Jacques, B. Michaela, T. Alphonse and L. Cissá, Determination of the First Excited Singlet State Dipole Moments of Coumarins by the Solvatochromic Method, Spectrosc. Lett., 1994, 27, 439–449.

63 A. Golonko, H. Lewandowska, R. Świsłocka, U. T. Jasińska, W. Priebe and W. Lewandowski, Curcumin as tyrosine kinase inhibitor in cancer treatment, Eur. J. Med. Chem., 2019, 181, 111512.

64 K. Bozali, E. Güler and M. Çelikten, Investigation of the effect of curcumin on cytotoxicity, genotoxicity, and apoptosis on breast cancer cells, World Cancer Research J., 2022, 9, e2149.

65 J. A. McCubrey, K. Lertpiriyapong, L. S. Steelman, S. L. Abrams, L. V. Yang, R. M. Murata, P. L. Rosalen, A. Scalisi, L. M. Neri, L. Cocco, S. Ratti, A. M. Martelli, P. Laidler, J. Dulińska-Litewka, D. Rakus, A. Gizak, P. Lombardi, F. Nicoletti, S. Candido, M. Libra, G. Montalto and M. Cervello, Effects of resveratrol, curcumin, berberine and other nutraceuticals on aging, cancer development, cancer stem cells and microRNAs, *Aging*, 2017, **9**, 1477–1536.